American Mineralogist, Volume 97, pages 1653–1661, 2012

The sulfur speciation in S-bearing minerals: New constraints by a combination of electron microprobe analysis and DFT calculations with special reference to sodalite-group minerals

Kai Hettmann,* Thomas Wenzel, Michael Marks, and Gregor Markl

Fachbereich Geowissenschaften, Eberhard-Karls Universität Tübingen, Wilhelmstrasse 56, 72072 Tubigen, Germany

Abstract

In this work, we present an improved method for the semi-quantitative determination of sulfur species in S-bearing minerals by electron microprobe analysis. For calibration, we analyzed several sulfate and sulfide standard minerals such as baryte, celestine, chalcopyrite, and pyrite, and correlated the results with theoretical calculations retrieved from density functional theory (DFT). We applied this method to natural sodalite-group minerals from various localities. In addition, we applied the more common Raman spectroscopy to some samples and show that this method cannot be applied to sodalite-group minerals to determine their sulfur speciation. We show that even though sodalite-group minerals have a complex crystal structure and are sensitive to the electron beam, electron microprobe analysis is a reliable tool for the analysis of their sulfur speciation. The natural sodalite-group minerals show systematic variations in sulfur speciation. These variations can be correlated with the independently determined oxidation state of the parental magmas thus making S-bearing sodalite-group minerals good redox proxies, although we show that the electron microprobe analysis of the sulfur speciation is matrix-dependent, and the sulfur speciation itself depends on crystal chemistry and structure, and not only on f_{O_2}.

Keywords: Sulfur speciation, igneous, sodalite, oxygen fugacity, electron microprobe, Raman spectroscopy, density functional theory

Introduction

The analysis of redox-sensitive elements attracts much attention in geosciences because the redox state is an important intensive parameter. In addition to iron and carbon, sulfur is one of the most common redox-sensitive elements in nature (Behrens and Webster 2011).

Carroll and Rutherford (1988) used an electron microprobe (EMP)-based method to determine the sulfur speciation in basaltic glasses, but did not consider systematical errors due to standardization. Mori et al. (2009) used X-ray emission spectroscopy to study the oxidation state of sulfur in synthetic materials and showed a good correlation between the energy of the $K\alpha_{1,2}$ X-ray line and the charge of natural and synthetic sulfur-bearing solids calculated by density functional theory. Several studies using a broad range of methods have been utilized to investigate the sulfur speciation of sodalite-group minerals (SGM) and synthetic equivalents (Di Muro et al. 2004; Gobeltz-Hautecoeur et al. 2002; Lede et al. 2007; Bellatreccia et al. 2009; Hassan 2000; Fleet 2005; Fleet et al. 2005; Goslar et al. 2009). However, the methods used are mostly time-consuming and not easily accessible, whereas EMP analysis is commonly used in geosciences, and offers a very good spatial resolution of a few cubic micrometers. Here, we present an approach to determine sulfur speciation in SGMs using EMP analysis (cf. Carroll and Rutherford 1988). We combine these analyses with DFT calculations because good correlations between calculated atomic charges and bonding properties and related changes in the X-ray emission spectra are seen in these calculations (Segall et al. 1996; Mori et al. 2009). Furthermore, we compare Raman spectra of natural samples with theoretically predicted spectra to assign the observed Raman bands to specific vibration modes of different anions. This allows us to explore the possibilities of quantification of the content of sulfur species in SGM by Raman spectroscopy.

Density functional theory allows the prediction of the electronic structure of theoretical compounds (Giannozzi et al. 2009). The electronic structure with the lowest energy is calculated iteratively by solving the Schrödinger equation for the electrons, using the electron density to approximate the electron-electron interactions. The resulting electronic structure can be used to calculate other properties like atomic charges of the constituting atoms and vibrational energies.

Sodalite-group minerals are common in alkaline magmatic, hydrothermal, and some rare meta-evaporitic rocks (e.g., Hogarth and Griffin 1976; Di Muro et al. 2004; Suk et al. 2007; Markl et al. 2010). They have a zeolite-like cubic structure with two structural cavities per unit cell (van Peteghem and Burley 1963; Merlino 1984; Fischer and Bauer 2009). The structural framework is made up by silica-, alumina-, or beryllium-tetrahedra with inter-framework sites either occupied by Na and Ca or by Fe, Mn, and Zn (see Fig. 1; for an overview on SGM end-members see Table 1). Solid solutions are known to be common between the Na- and Ca-bearing end-members (van Peteghem

* E-mail: kai.hettmann@uni-tuebingen.de

0003-004X/12/0010–1653$05.00/DOI: http://dx.doi.org/10.2138/am.2012.4031

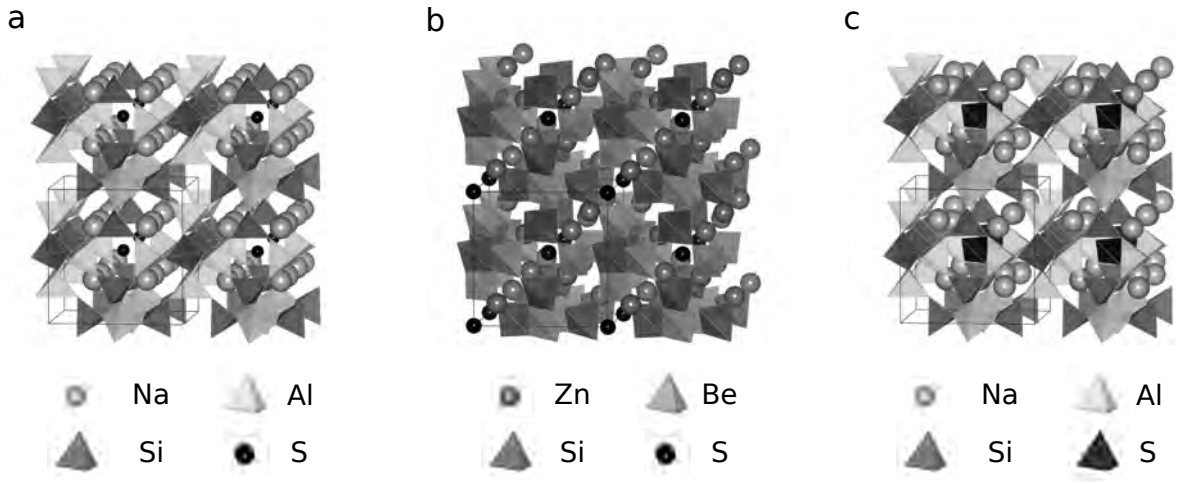

FIGURE 1. Crystal structures of sulfur-bearing sodalite-group minerals as calculated by DFT (this study): (**a**) lazurite; (**b**) genthelvite; (**c**) nosean. The colors for the elements are shown in the legend, and O atoms are not shown, but incorporated into tetrahedra.

TABLE 1. Overview of the endmembers of the sodalite-group

End-member	Formula
sodalite-subgroup	
sodalite	$Na_8Al_6Si_6O_{24}Cl_2$
nosean	$Na_8Al_6Si_6O_{24}SO_4$
hauyne	$Na_6Ca_2Al_6Si_6O_{24}(SO_4)_2$
lazurite	$Na_8Al_6Si_6O_{24}S$
tugtupite-subgroup	
tugtupite	$Na_8Be_6Si_6O_{24}Cl_2$
danalite-subgroup	
danalite	$Fe_8Be_6Si_6O_{24}Cl_2$
genthelvite	$Zn_8Be_6Si_6O_{24}Cl_2$
helvite	$Mn_8Be_6Si_6O_{24}Cl_2$

and Burley 1963; Taylor 1986; Di Muro et al. 2004), excluding the rare tugtupite (for which no data on solid solutions exist), and between the Fe-, Mn-, and Zn-bearing end-members (Hassan and Grundy 1985).

The structural cavities are usually occupied by chlorine, sulfur species, carbonate, or molecular water (e.g., Kotelnikov et al. 2005; Bellatreccia et al. 2009; Fleet et al. 2005). The two important sulfur species in natural SGMs are sulfate (SO_4^{2-}) and sulfide (S^{2-}) (Fleet et al. 2005), which can continuously substitute for each other (Hassan 2000; Wulff-Pedersen et al. 2000). The sulfate/sulfide ratio can in principle be used to investigate the redox conditions during their formation (Carroll and Rutherford 1988; Markl et al. 2010), since reactions between sulfide and sulfate species are f_{O_2} dependent. In addition, the formation of sodalite itself can have a major influence on volatile contents and on the redox state of peralkaline melts (Stormer and Carmichael 1971; Markl et al. 2010).

SAMPLE DESCRIPTIONS

Anhydrite ($CaSO_4$), baryte ($BaSO_4$), celestine ($SrSO_4$), galena (PbS), and molybdenite (MoS_2) from the MINM25-53 Astimex Scientific Limited mineral mount and chalcopyrite ($CuFeS_2$), covellite (CuS), and pyrite (FeS_2) from a Micro Analytical Consultants mineral mount (Std.-Nr. 4569) were used for the calibration of the EMP.

Natural SGM samples analyzed after the calibration procedure were taken from collections of the authors. They come from the Ilímaussaq magmatic complex, southwest Greenland (the type locality of sodalite), the Laacher See volcanics, Germany (the type locality of nosean), the magmatic Mont Saint-Hilare complex, Canada, and from a meta-sedimentary rock series from Afghanistan. One historical sample labeled as "Lasurstein" from "Persia" (most probably from Afghanistan) was taken from the mineral collection of the University of Tübingen. The samples from the Ilimaussaq intrusion include sodalite and helvite, the samples from Laacher See nosean and hauyn, the samples from Mont Saint-Hilare sodalite and the sample from Afghanistan lazurite. The sodalite samples from the Ilímaussaq intrusion are cumulus crystals (~5 mm in diameter) from an agpaitic nepheline syenite, whereas the helvite sample is a euhedral crystal (~2 mm in diameter) from a hydrothermal microcline-rich vein. The sodalite from Mont Saint-Hilare is from a nepheline syenite and euhedral with ~2 mm diameter. The Laacher See samples are euhedral crystals of about 2 mm in a fine-grained volcanic matrix. The samples from Afghanistan and "Persia" are blue aggregates in a fine-grained metamorphic rock, consisting of SGM, pyrite, and carbonates. The SGM in these samples are very fine-grained at a scale of about 50 µm.

ANALYTICAL APPROACH

Electron microprobe (EMP) analysis

Analyses were performed at Tübingen University using a JEOL 8900 Superprobe with 15 kV acceleration voltage and 20 nA beam current. A focused beam was used for sulfate and sulfide standard minerals whereas a 20 µm probe diameter was used for SGM minerals to prevent destruction and loss of Na. Test analyses in the course of this study on baryte did not show any significant variations in the peak position of the S$K\alpha_{1,2}$ X-ray line of the standard materials in relation to variations in beam diameter, beam current or acceleration voltage. The emitted X-rays were detected using pentaerythritol (PET) crystals combined with an XCE-type and an H-type wavelength-dispersive X-ray spectrometer, respectively. The smallest available detector slit of 300 µm was used at the XCE-type spectrometer, while the H-type spectrometer has a fixed detector slit of 500 µm. The crystals were scanned with a step size of 4 µm corresponding to a change in energy of ~0.05 eV every 8 s. To reduce the total measurement time, only the central part of the S$K\alpha_{1,2}$ X-ray line between 2304.96 and 2312.32 eV was recorded (see Fig. 2). The resulting spectrum was fitted with a pseudo-Voigt function, because these functions are ideal for the interpretation of wavelength-dispersive spectra (Remond et al. 2002). These fits are in good agreement with the acquired data in the complete energy

range shown in Figure 2. The maxima estimated from these data are identical within error with the maxima estimated by applying the fit to the restricted energy range (gray area in Fig. 2).

We observed small variations of the S$K\alpha_{1,2}$ peak position with time, which is related to small temperature fluctuations in the lab (within 2 °C) causing thermal expansion of the PET crystal (Barrio et al. 1994). This expansion is significant in relation to the variations in peak position observed in the samples. To correct for these "artificial" variations, sphalerite was analyzed before and after each analysis. The fitted peak positions were then corrected to a sphalerite peak position of 2307.56 eV for the XCE-type spectrometer and 2308.19 eV for the H-type spectrometer. The resulting uncertainty was calculated from five sequential bracketing analyses (given as 2σ in Tables 2 and 3).

Raman spectroscopy

The Raman spectra were obtained using a Renishaw InVia Reflex μ-Raman spectrometer. The laser had a wavelength of 532 nm, was focused with a backscattering geometry and analyzed with an 1800 L/mm grating. An edge filter and a 50× object lens (numerical aperture 0.55) were used, resulting in a ~2 μm spot size. The samples have been analyzed in arbitrary orientation since the scope of this study was the in situ analysis of the sulfur speciation. Orientation of the samples was not possible due to practical difficulties.

Theoretical calculations

Theoretical calculations were performed using the plane wave electronic structure package QUANTUM ESPESSO (Giannozzi et al. 2009) carried out at the computational facilities of the bwGRiD project at the University of Tübingen, Germany. In particular, we performed calculations on the atomic charge of sulfur in various mineral phases including baryte, sphalerite, celestine, pyrite, galena, nosean, lazurite, and Zn-bearing genthelvite. Zn-bearing genthelvite was used, because helvite is Mn-bearing and the electronic structure of Mn is not well described using density functional theory. Calculations were performed using the generalized gradient approximation (GGA) within the PBE exchange correlation formalism (Perdew et al. 1996), which takes the electron density and its gradient at each point into account. Ultrasoft pseudopotentials were employed, excluding semicore *s*- and *p*-states for Na and Al. Cutoffs and the number of **k**-points were tested for convergence. The charge of the atoms was calculated using Löwdin

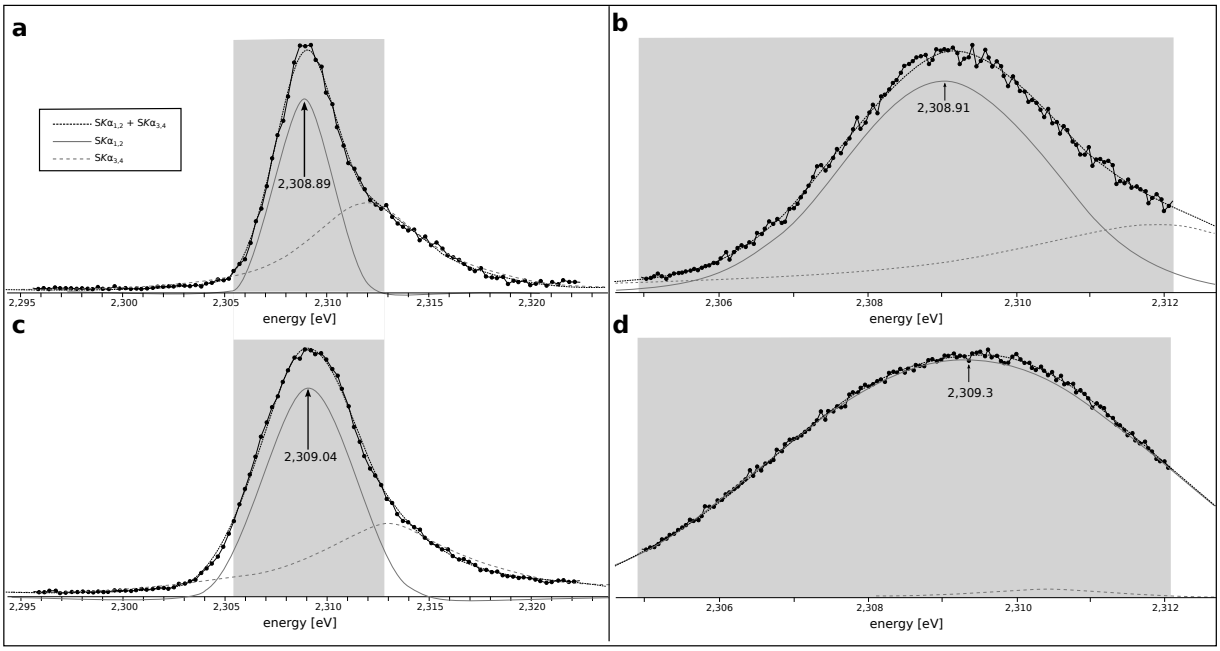

FIGURE 2. S$K\alpha_{1,2}$ X-ray spectra of a nosean sample (KHSO4) detected by a PET crystal in an XCE-type spectrometer (**a** and **b**) and an H-type spectrometer (**c** and **d**), respectively. For comparison, complete peaks at a lower resolution (**a** and **c**) and the energy range used at a higher resolution (**b** and **d**) are shown.

TABLE 2. Analyses of standard materials and results of theoretical calculations on end-members

Mineral	Chemical formula	Sulfur $K\alpha_{1,2}$ peak positions (eV ± 2σ)		DFT atomic charge
		XCE-type spectrometer	H-type spectrometer	
		Sulfides		
chalcopyrite	$CuFeS_2$	2307.76 ± 0.08	2307.56 ± 0.02	not calculated
covellite	CuS	2307.79 ± 0.11	2307.58 ± 0.06	not calculated
galenite	PbS	2307.55 ± 0.06	2308.16 ± 0.10	6.29
genthelvite	$Zn_8Be_6Si_6O_{24}S_2$	see Table 3	see Table 3	6.72
lazurite	$Na_8Al_6Si_6O_{24}S$	see Table 3	see Table 3	4.62
molybdenite	MoS_2	2307.82 ± 0.04	2307.55 ± 0.02	not calculated
sphalerite	ZnS	2307.79 ± 0.07	2307.61 ± 0.03	7.13
		Polysulfides		
pyrite	FeS_2	2307.84 ± 0.06	2307.59 ± 0.04	5.91
		Sulfates		
anhydrite	$CaSO_4$	2308.84 ± 0.01	2309.46 ± 0.20	not calculated
baryte	$BaSO_4$	2309.24 ± 0.04	2308.91 ± 0.05	2.82
celestite	$SrSO_4$	2309.17 ± 0.14	2309.71 ± 0.24	2.73
nosean	$Na_8Al_6Si_6O_{24}SO_4$	see Table 3	see Table 3	3.57

TABLE 3. Results of the analysis of natural samples

Sample	Locality	Sulfur $K\alpha_{1,2}$ peak positions [eV ± 2σ]	
		XCE-type spectrometer	H-type spectrometer
		Hauyn	
KHSO3	Laacher See	2309.02 ± 0.05	2309.34 ± 0.01
		Helvite	
KH99	Ilímaussaq	2307.68 ± 0.10	2308.29 ± 0.02
		"Lazurite"	
KHSO5	Afghanistan	2308.98 ± 0.05	2309.02 ± 0.11
KHSO2	"Persia"	2309.10 ± 0.06	2308.98 ± 0.11
		Nosean	
KHSO4	Laacher See	2309.10 ± 0.16	2309.31 ± 0.03
		Sodalite	
GM1369	Ilímaussaq	2308.43 ± 0.04	2308.25 ± 0.07
GM1344	Ilímaussaq	2308.23 ± 0.05	2308.44 ± 0.11
MH45	Mont-Saint Hilaire	2308.74 ± 0.15	2308.73 ± 0.07
MH90	Mont-Saint Hilaire	2308.74 ± 0.05	2308.73 ± 0.06

analysis (Löwdin 1977). The calculated crystal structure and atomic positions of all investigated phases (for the SGM see Fig. 1) were compared to the IMA-accepted experimental values and show agreement within 10% for the lattice parameters.

In addition, Raman spectra for the sodalite and nosean end-members have been calculated using the same software [see Baroni et al. (2001) and Lazzeri and Mauri (2003) for details]. The vibrational energies are calculated from the first- and second-order derivatives of the potential energy surface of the electron density. In contrast to the calculation of the atomic charges, this has been executed using the local density approximation (LDA) (Perdew and Zunger 1981), which only takes the electron density at each point into account, and norm-conserving pseudopotentials, because the calculation of Raman spectra is not implemented for the method used above. Again cutoffs and the number of **k**-points were tested for convergence and for a theoretical sulfide-bearing end-member of SGM no convergence in the phonon calculation was reached. The spectra have been calculated by using Gauss distributions on each theoretical band. The calculations include the forces acting on every atom in each band, which can be used to attribute all bands to specific vibrations.

RESULTS

EMP analysis of sulfate and sulfide standard minerals

The S$K\alpha_{1,2}$ peak position varies within two distinct groups. The first group includes the analyzed sulfide minerals galena, molybdenite, chalcopyrite, covellite, and pyrite, and is restricted to an energy range between 2307.55 eV for molybdenite and 2308.16 eV for galena on the H-type spectrometer (see Fig. 3a and Table 2). The analyses on the XCE-type spectrometer show slightly lower energies between 2307.55 eV for galena and 2307.82 eV for molybdenite (see Fig. 3a and Table 2). In contrast, the analyzed sulfate minerals show significantly higher energies of the $K\alpha_{1,2}$ peak positions. They range from 2308.84 eV for anhydrite to 2309.24 eV for baryte using the H-type spectrometer. Analytical results produced by the XCE-type spectrometer show a larger spread between 2308.91 eV for baryte and 2309.71 eV for celestine (see Fig. 3a and Table 2).

Theoretical calculations of the atomic charge of sulfur species in different minerals

Calculations for the atomic charge of sulfur were performed for baryte, sphalerite, celestine, pyrite, and galena and for the sulfur-bearing end-members of the sodalite-group minerals nosean, lazurite, and genthelvite. The calculated atomic charges represent the partial amount of the outer electrons (3*s* and 3*p*), which can be attributed to the sulfur atom. They are representative of the valence state and the bonding properties of sulfur in the analyzed minerals (Segall et al. 1996).

Again two distinctive groups namely sulfidic and sulfatic phases (see Fig. 3b and Table 3) emerged. Sulfides and sulfide-bearing phases have more electrons attributed to the sulfur atom than sulfates: the number of 3*s*- and 2*p*-electrons range from 5.91 in pyrite to 7.12 in sphalerite. On the other hand, the sulfur atom in the sulfidic sodalite-end-member lazurite has only 4.62 3*s*- and 2*p*-electrons. In genthelvite, sulfur has 6.72 3*s*- and 2*p*-electrons. The sulfur in the sulfate-bearing phases has distinctively less 3*s*- and 2*p*-electrons attributed to the sulfur atom: 2.74 for celestine to 2.82 for baryte and 3.57 in the sulfate-bearing sodalite end-member nosean.

EMP analysis of SGM samples

The natural samples analyzed in this study produce significantly lower intensities of the S$K\alpha_{1,2}$ X-ray line than the standards, because of their lower sulfur concentrations. In some analyses of chlorine-dominated sodalite samples, no clear peak could be observed in the data obtained by the XCE-type spectrometer. In very few analyses (not shown on figures), even a clear peak also could not be observed in the data from the H-type spectrometer. Quantitative analysis showed that the lowest sulfur concentrations in samples, where at least one peak could

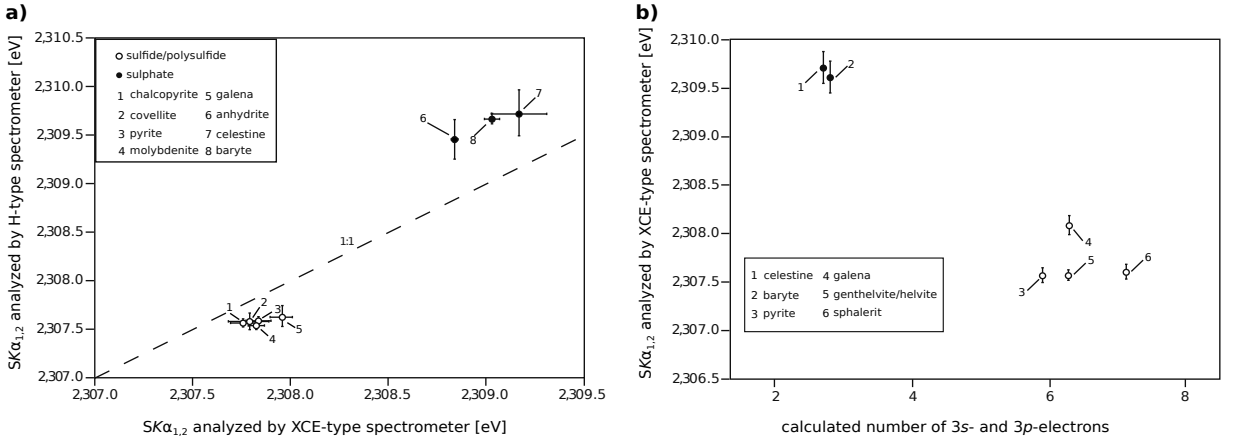

FIGURE 3. (**a**) Comparison of S$K\alpha_{1,2}$ peak positions of standard minerals analyzed by an XCE- and an H-type spectrometer, respectively. (**b**) Comparison of S$K\alpha_{1,2}$ peak positions analyzed by an XCE-type spectrometer with calculated numbers of 3*s*- and 3*p*-electrons.

be observed, is about 2000 ppm.

The observed S$K\alpha_{1,2}$ peak positions show a large spread. Nosean from the Laacher See volcanics has a S$K\alpha_{1,2}$ peak position of 2309.10 ± 0.16 and 2309.31 ± 0.03 eV for H- and XCE-type spectrometer, respectively (see Fig. 3a). Hauyn from the same locality gives results within an identical range (2309.02 ± 0.05 and 2309.34 ± 0.01 eV). The S$K\alpha_{1,2}$ X-ray line of the helvite sample, in contrast, has distinctively lower energies. It has peak positions of 2307.68 ± 0.10 and 2308.29 ± 0.02 eV, respectively (see Fig. 3a). The sodalite samples showed peak positions between 2308.25 and 2308.74 eV using the H-type spectrometer and between 2308.87 and 2309.06 eV using the XCE-type spectrometer (see Fig. 3a). Various samples from identical localities show reproducible and distinctive S$K\alpha_{1,2}$ peak positions. The highest energies we found are associated with samples from "Persia" and Afghanistan, intermediate energies are associated with samples from Mont Saint-Hilare, Canada, and the lowest energies are associated with samples from Ilímaussaq, southwest Greenland.

Raman spectroscopy

Two kinds of Raman spectra have been obtained in the course of this study, theoretically predicted spectra and experimental spectra of natural samples, both for sodalite and nosean. The spectra for sodalite match well (see Figs. 4a and 4c): all predicted bands occur in the analyzed spectra within 50 cm^{-1} in Raman-shift and are in good agreement with the predicted relative intensity. Overall, the spectra show two major groups of bands, one in the range between 200 and 500 cm^{-1}, and the other one between 900 and 1150 cm^{-1}. The two most intensive bands in both spectra are at ~450 cm^{-1} and slightly below 1000 cm^{-1}. The theoretical spectrum for nosean shows less agreement with the spectrum of the natural sample (see Figs. 4b and 4d). However, most bands observed in the natural sample can be related to the theoretically predicted bands. The overall spectra show similarities to the sodalite spectra, again with two major groups of bands between 200 to 500 cm^{-1} and between 900 and 1150 cm^{-1}. In contrast to the sodalite spectra the most intensive band in the theoretical spectra is at ~920 cm^{-1}, but the second most intensive band is again slightly below 1000 cm^{-1}.

Discussion

Analytical parameters of the EMP

The determination of the oxidation state of sulfur in SGMs is non-trivial since their sulfur content can reach levels below the detection limit of classical EMP analysis in some samples. Furthermore, SGMs are frequently affected by low-temperature (hydrothermal) alteration, which results, for example, in the partial reaction to zeolites, and may also change the sulfur speciation. This effect of secondary alteration can only be excluded if in situ methods with high spatial resolution are used. Hence, SGM sulfur analysis requires a method with relatively low limits of detection and high spatial resolution, which should preferably be relatively quick, easily available, and inexpensive, to enable its usage routinely. All these arguments support the use of the electron microprobe.

Since sodalite is a mineral that can be damaged by long-time

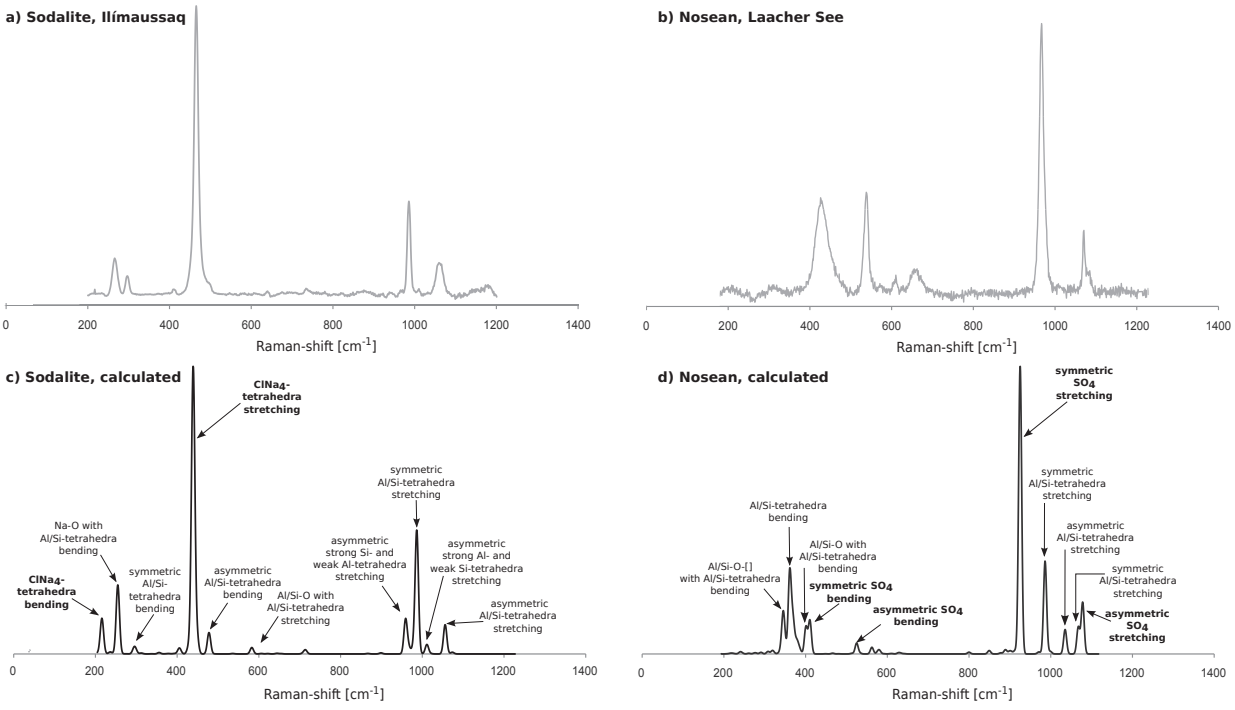

Figure 4. Raman spectra of sodalite (**a** and **c**) and nosean (**b** and **d**), theoretically predicted (**a** and **b**) and real spectra acquired on natural samples (**c** and **d**) are shown. The bands related to anions in the structural cavities are labeled in bold.

exposure to an electron beam (Johnson et al. 1978), the measurement time has to be minimized. In this work, this has been achieved by restricting the analyzed energy range. Furthermore, we used both the H-type and an XCE-type spectrometer. The H-type spectrometer detects signals of low intensity better than an XCE-type spectrometer, resulting in higher count rates. In contrast, the XCE-type spectrometer has a higher energy resolution than the H-type spectrometer. Using this combination renders it possible to analyze SGM samples with sulfur contents as low as 2000 ppm, which is higher than the detection limit of Raman spectroscopy on magmatic glasses (Wilke et al. 2011). However, the detection limit in Raman spectroscopy is strongly dependent on the fluorescence, which is extremely high in SGM (Klimm and Botcharnikov 2010).

We emphasize that the S$K\alpha_{1,2}$ X-ray shift due to thermal variations during analysis has to be monitored and corrected for, since they are significant in relation to the high-energy resolution required. For this reason, all analyses have to be performed by the standard bracketing method. If all these factors are taken into account, the analysis of the sulfur speciation by electron microprobe provides reproducible and at least semi-quantitative results. However, in the case of SGM we expect differing positions for different end-members (e.g., helvite) and therefore theoretical calculations need to be taken into account (see below).

Combining DFT calculations and EMP analytical results

Theoretical predictions on the charge of sulfur atoms in various natural and synthetic compounds showed a good correlation with X-ray emission spectroscopic results (Mori et al. 2009). We observe the same relationship in our study for the electron microprobe analyses of standard materials (see Fig. 3a). It is interesting to note, however, that pyrite does not strictly follow this relationship. This is caused by the fact that pyrite does not contain simple sulfidic sulfur but the polysulfide S_2^{2-} ion (Mori et al. 2009). This difference causes changes in the electronic fine-structure of the S$K\alpha_{1,2}$ X-ray line not resolvable by electron microprobe. However, simple sulfate (SO_4^{2-}) and sulfide (S^{2-}) anions, which are much more common in nature (Fleet et al. 2005), show a simple relationship with the theoretical charge predictions. This relationship can be used to "calibrate" other sulfur-bearing phases by inferring the end-member peak-positions from the calculated charge of the sulfur atom.

However, theoretical predictions show that sulfidic sulfur in SGMs has atomic charges differing from sulfur in simple sulfide materials. The charge differs significantly between the Fe/Mn/Zn- and the Na-bearing end-members. To our knowledge no solid solution between the Fe/Mn/Zn- and Na/Ca-bearing end-members is known to exist and the occupation of the structural cavities differs (in the Fe/Mn/Zn-bearing end-members both structural cavities are occupied by sulfide anions to maintain charge balance, whereas only one is occupied by sulfide anions in the Na/Ca-bearing end-members), therefore we treat Fe/Mn/Zn- and Na/Ca-bearing end-members differently. Since no standard materials of sulfide-bearing sodalite-group minerals are available, we chose to use the theoretical predictions to calibrate our analytical procedure using the calculated atomic charges of sulfur. This leads to the conclusion that the position of the S$K\alpha_{1,2}$ X-ray line differs between Na/Ca- and Fe/Mn/Zn-bearing sodalite-group minerals. The position of the S$K\alpha_{1,2}$ X-ray line in Fe/Mn/Zn-bearing sodalite-group minerals is in the same range as the one of other phases containing sulfidic sulfur such as chalcopyrite and galena. In contrast, the position of the S$K\alpha_{1,2}$ X-ray line in Na/Ca-bearing sodalite-group minerals shows an offset to higher energies, which would cause an underestimation of the sulfidic sulfur, if only simple sulfide mineral standards are used and no calculation would correct for it.

Raman spectroscopy of natural samples and DFT results

The theoretical spectra obtained by DFT allow the assignment of vibrational modes to each band occurring in the Raman spectra (see Figs. 4 c and 4d). In both cases (sodalite and nosean) we can distinguish three different groups of vibrational modes. Vibrational modes of the first group are related to bending of Al- and Si-tetrahedra. The related bands are situated between 200 and 500 cm^{-1} and occur in sodalite and nosean spectra at different positions.

The second group consists of vibrational modes related to the stretching of Al- and Si-tetrahedra, and comprise of bands between 900 and 1150 cm^{-1}. Again this is true for both the sodalite and the nosean spectra. The positions of these two types of vibrational modes are typical for silicates in general (Furukawa et al. 1981).

In contrast, the third group differs between both minerals, because they are related to the anions in the structural cavity; chlorine in sodalite and sulfate in nosean. In both cases, two bands can be attributed to them, one related to bending (at lower wavenumbers) and one related to the stretching (at higher wavenumbers) of $ClNa_4$- and SO_4-tetrahedra. For the sodalite end-member, the $ClNa_4$-tetrahedron bending and stretching bands occur at ~220 and ~450 cm^{-1}, respectively. In end-member nosean, the bending modes for SO_4 occur at ~420 and ~520 cm^{-1}, respectively, and the stretching modes at ~900 and ~1100 cm^{-1}.

If the theoretical spectra are compared with the spectra of the natural samples, there is a good agreement for sodalite, but a mismatch for some bands in the nosean spectra. Although the general band distribution for the natural sample (Fig. 4b) is similar to that of the calculated end-member (Fig. 4d), we see a strong broadening of the band at around 430 cm^{-1} in the natural spectrum, whereas several bands occur in the theoretical spectrum in this region. This mismatch can be explained by the discrepancy of the half-width in the analytical setup, which is affected by temperature, small distortions due to minor components (e.g., Mohanan et al. 1993), isotopic broadening (e.g., Hass et al. 1992), and the assumption of the same empirical half-width for all bands for the theoretically predicted spectra.

There are also bands that occur in the spectrum of the natural sample that cannot be clearly correlated to the theoretical spectrum without assuming strong shifts of the band energies. These shifts might be caused by minor elements, especially Li and K, in the nosean sample. The incorporation of Li and K into a Zeolith A framework (very similar to the SGM structure) leads to a band shifted to higher energies compared to the Na-band (Dutta and del Barco 1985). In addition, the occupation of the nominally unfilled cavity might particularly cause structural changes, as has been shown for the dehydration of sodalite-like zeolites (Brémard and Bougeard 1995). The cavity can be oc-

cupied by minor chlorine, which causes the occupation of two cavities per unit cell and associated structural changes, as we see if we compare the spectra of sodalite and nosean. The structural cavity can also be occupied by, e.g., molecular water, nitrogen and carbon species, which all might cause structural changes and therefore changes in the Raman spectrum. The mismatch in band intensities can be explained by polarization effects, which cause variations in the band intensities depending on the orientation of a crystal (e.g., Ishibashi et al. 2008).

The mismatch in the Raman spectra has no direct consequences for this study on the sulfur incorporation since the identification of bands related to sulfur species was unambiguously possible, which is the major scope of this investigation, and it is shown that the analysis of the sulfur speciation in sodalite is not possible with Raman spectroscopy.

Comparing EMP and Raman spectroscopy

For SGM, the speciation of sulfur can be analyzed by electron microprobe semi-quantitatively. In contrast, the comparison between theoretical and actual Raman spectra shows that, even though this technique has been shown to result in a higher precision and almost the same lateral resolution (ignoring the penetration depth), it cannot easily be applied to SGM, because the only intensive sulfate-related band overlaps with Si/Al-tetrahedra-related bands. Raman-spectroscopy, therefore, cannot be used to quantify the amount of sulfate in sulfur-poor SGM and consequently it is impossible to determine the speciation of sulfur. In the natural sodalite from Ilímaussaq none of the observed bands correlate to sulfur in any chemical mode.

The sulfur speciation in natural sodalite-group minerals

Natural SGM samples analyzed in this study show large variations in their sulfur content and in their sulfur speciation. Samples from the Laacher See volcanics, "Persia" and Afghanistan contain pure sulfate sulfur, while sodalites from Mont Saint-Hilare contain mixed sulfide and sulfate sulfur, and the samples from Ilimaussaq show the highest contents of sulfide sulfur clearly dominating over sulfate. The helvite sample analyzed in this study, finally, contains no detectable sulfate and is hence a purely sulfidic SGM. Since the size of the structural cavity in Fe/Mn/Zn-bearing SGMs is much smaller than in Na/Ca-bearing ones, we interpret our finding such that these minerals can only incorporate sulfidic sulfur. Hence, in Fe/Mn/Zn-SGMs, sulfur analysis cannot be related to the redox state of the melt or fluid from which they crystallize. In the Na/Ca-bearing sodalite-group minerals, in contrast, we found both sulfide and sulfate, and we will show below that their sulfate/sulfide ratio is a monitor of the redox conditions of the melt or fluid they formed from. Although sulfide-rich samples in our study are all chlorine-dominated, several other authors have reported sulfide-dominated Cl-poor Na/Ca-bearing SGMs (e.g., Hassan et al. 1985; Fleet 2005; Fleet et al. 2005). Hence, our results are regarded as sample bias rather than reflecting a deeper principle.

The magmatic samples used in this study show a correlation of sulfate/sulfide ratios in SGM with previously and independently determined oxidation states of the respective magmas. The Laacher See volcanics are oxidized and crystallized at ΔNNO+1 (Harms et al. 2004). As would be expected, our SGM samples from this locality are dominated by sulfate (Fig. 5). The samples from Mont Saint-Hilaire crystallized under slightly reducing conditions of ΔFMQ-1 (Schilling et al. 2011), and their SGMs contain ~1:1 sulfide and sulfate. The samples from Ilimaussaq, which formed in one of the most reduced magmas known on Earth (ΔFMQ-1 to -4; Markl et al. 2001), contain only sulfide. Hence, sulfate/sulfide ratios monitor the oxidation state of the magma the SGMs crystallized from, but in a different way than sulfate/sulfide-ratios of glasses (see Fig. 6). If we compare the sulfur speciation ratio of experimental basaltic melts quenched at variable oxidation conditions with our estimations on sodalite, the sodalite speciation curve is shifted to lower oxygen fugacities by about 2 log units (Wilke et al. 2011). The same shift has been shown for Na-silicate melts (Nagashima and Katsura 1973; Jugo et al. 2005). Since Na-bearing SGM have basically the same composition, with varying anions in the structural cavity and sometimes with minor Ca, this effect can be attributed to the presence of high Na-concentrations. This indicates that sulfate is relatively more stable than sulfide in Na-rich melts compared to basaltic melts. This observation shows that the dependence of the redox state of sulfur on oxygen fugacity is matrix-dependent. This also implies a change in the redox-conditions of a basaltic melt if Na-bearing SGM crystallizes as predicted by Markl et al. (2011). The SGM have a higher S^{6+}-content than the melt, which therefore gets more reduced during this process. In contrast, we did not find any sulfate in Fe/Mn/Zn-bearing SGM. This can be explained by the differences in the crystal structure, because Fe/Mn/Zn-bearing SGM have smaller cell parameters and smaller structural cavities. Since the sulfate anion is larger than the sulfide anion, this observation explains that sulfidic sulfur is more stable than sulfate. The comparison of all these data sets shows that there are two different kinds of matrix-dependencies: first, a dependence on the chemical composition and, second, a dependence on structural differences.

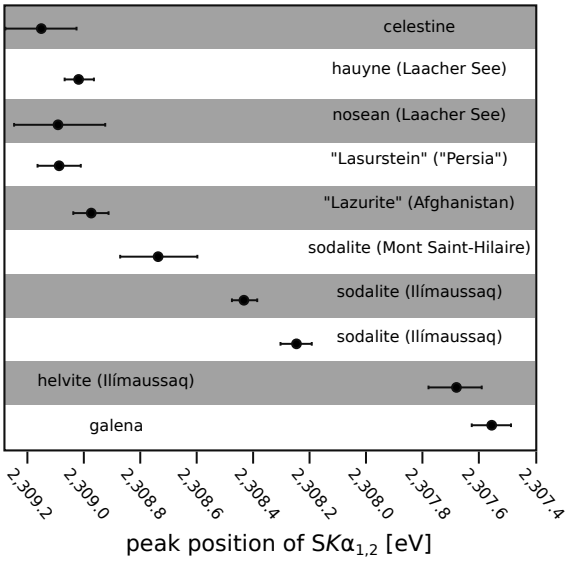

FIGURE 5. S$K\alpha_{1,2}$ peak positions of natural SGM minerals analyzed by an XCE-spectrometer. Selected standard materials are shown for orientation.

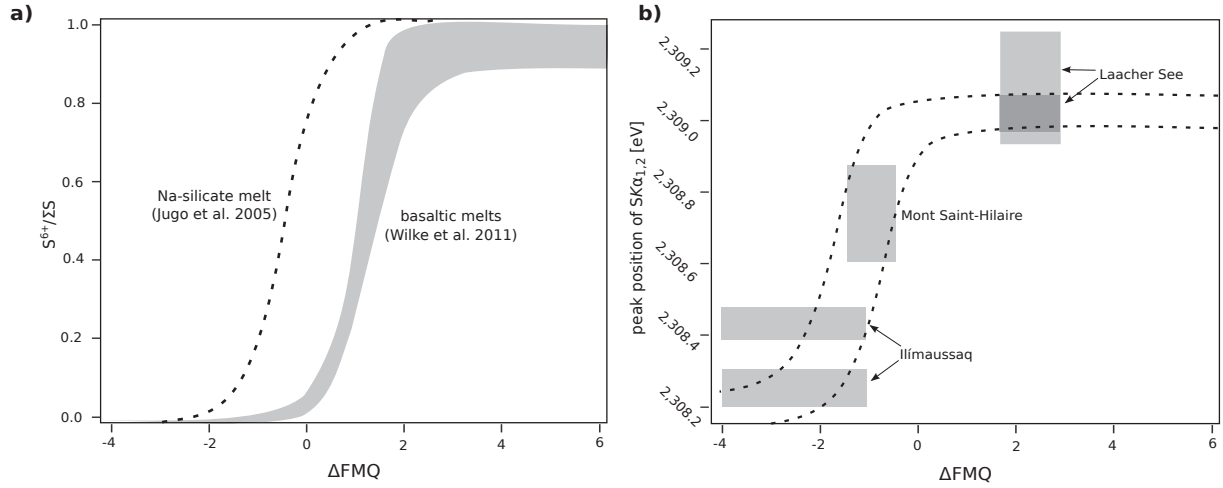

FIGURE 6. (**a**) Literature data on the sulfur speciation of experimental melts. (**b**) Comparison of S$K\alpha_{1,2}$ peak positions and published data on the oxygen fugacity of parental melts.

ACKNOWLEDGMENTS

We thank A. Kronz and H. Bohse for providing sample material, M. Keuper, L. Nasdala, and M. Nowak for their help with Raman spectroscopy, and J. Börder from JEOL Deutschland Ltd. for comments on the electron microprobe part. I. Derrey and F. Thaler provided valuable practical help during the study. We also thank F. Larner for helping us to improve the language of the manuscript with her comments. We gratefully thank the bwGRiD project for the computational resources. bwGRiD (http://www.bw-grid.de) is a member of the German D-Grid initiative, funded by the Ministry for Education and Research (Bundesministerium für Bildung und Forschung) and the Ministry for Science, Research and Arts Baden-Württemberg (Ministerium für Wissenschaft, Forschung und Kunst Baden-Württemberg). Financial support for this study has been provided by the Landesgraduiertenförderung Baden-Württemberg to Kai Hettmann and by the Krupp Foundation through the Alfried Krupp Prize for Young University teachers to Gregor Markl. We thank two anonymous reviewers and the associate editor for their helpful comments, which helped to improve this manuscript.

REFERENCES CITED

Baroni, S., de Gironcoli, S., Dal Corso, A., and Giannozzi, P. (2001) Phonons and related crystal properties from density-functional pertubation theory. Reviews of Modern Physics, 73, 515–562.

Barrio, M., Font, J., Lopez, D.O., Muntasell, J., Tamarit, J.Ll., and Haget, Y. (1994) Thermal-expansion tensors of pentaerythritol (PE) and pentaglycerin (PG) and compositional deformation tensor of $PG_{1-x}PE_x$ molecular alloys. Journal of Applied Crystallography, 27, 527–531.

Behrens, H. and Webster, J.D. (2011) Studies of sulfur in melts – Motivations and overview. In H. Behrens and J.D. Webster, Eds., Sulfur in Magmas and Melts: Its importance for natural and technical processes, 73, p. 1–8. Reviews in Mineralogy and Geochemistry, Mineralogical Society of America, Chantilly, Virginia.

Bellatreccia, F., Della Ventura, G., Piccinini, M., Cavallo, A., and Brilli, M. (2009) H_2O and CO_2 in minerals of the haüyne-sodalite group: An FTIR spectroscopy study. Mineralogical Magazine, 73, 399–413.

Brémard, C. and Bougeard, D. (1995) Raman scattering in zeolites and molecular sieves. Advanced Materials, 7, 10–25.

Carroll, M.R. and Rutherford, M.J. (1988) Sulfur speciation in hydrous experimental glasses of varying oxidation states: results from measured wavelength shifts of sulfur X-ray. American Mineralogist, 73, 845–849.

Di Muro, A., Bonaccorsi, E., and Principe, C. (2004) Complex colour and chemical zoning of sodalite-group phases in a hauynophyre lava from Mt. Vulture, Italy. Mineralogical Magazine, 68, 591–614.

Dutta, P.K. and del Barco, B.D. (1985) Raman spectroscopic studies of zeolite framework. Hydrated zeolite A and the influence of cations. Journal of Physical Chemistry, 89, 1861–1864.

Fischer, R.X. and Bauer, W.H. (2009) Symmetry relationships of sodalite (SOD)-type crystal structures. Zeitschrift für Kristallographie, 224, 185–197.

Fleet, M.E. (2005) XANES spectroscopy of sulfur in earth materials. The Canadian Mineralogist, 43, 1811–1838.

Fleet, M.E., Liu, X., Harmer, S.L., and Nesbitt, H.W. (2005) Chemical state of sulfur in natural and synthetic lazurite by S *K*-edge XANES and X-ray photoelectron spectroscopy. The Canadian Mineralogist, 43, 1589–1603.

Furukawa, T., Fox, K.E., and White, W.B. (1981) Raman spectroscopic investigation of the structure of silicate glasses. III. Raman intensities and structural units in sodium silicate glasses. Jounal of Chemical Physics, 75, 3226–3238.

Giannozzi, P., Baroni, S., Bonini, N., Calandra, M., Car, R., Cavazzoni, C., Ceresoli, D., Chiarotti, G.L., Cococcioni, M., Dabo, I. and others. (2009) Quantum espresso: A modular and open-source software project for quantum simulations of materials. Journal of Physics: Condensed Matter, 21, 395502–395521.

Gobeltz-Hautecoeur, N., Demortier, A. Lede, B., Lelieur, P., and Duhayon, C. (2002) Occupancy of the sodalite cages in the blue ultramarine pigments. Inorganic Chemistry, 41, 2848–2854.

Goslar, J., Lijewski, S., Hoffmann, S.K., Jankowska, A., and Kowalak, S. (2009) Structrure and dynamics of S3-radicals in ultramarine-type pigment based on zeolite A: Electron spin resonance and electron spin echo studies. Journal of Chemical Physics, 130, 204504–204515.

Harms, E., Gardner, J.E., and Schmincke, H.-U. (2004) Phase equilibria of the lower Laacher See tephra (east Eifel, Germany): Constraints on pre-eruptive storage conditions of a phonolitic magma reservoir. Journal of Volcanology and Geothermal Research, 134, 125–138.

Hass, K.C., Tamor, M.A., Anthony, T.R., and Banholzer, W.F. (1992) Lattice dynamics and Raman spectra of isotopically mixed diamond. Physical Review B, 45, 7171–7182.

Hassan, I. (2000) Transmission electron microscopy and differential thermal studies of lazurite polymorphs. American Mineralogist, 85, 1383–1389.

Hassan, I. and Grundy, D. (1985) The crystal structures of helvite group minerals, $(Mn,Fe,Zn)_8(Be_6Si_6O_{24})S_2$. American Mineralogist, 70, 186–192.

Hassan, I., Petersen, R.C., and Grundy, H.D. (1985) The crystal structure of lazurite, ideally $Na_6Ca_2Al_6Si_6O_{24}S_2$, a member of the sodalite group. Acta Crystallographica, C41, 827–832.

Hogarth, D.D. and Griffin, W.L. (1976) New data on lazurite. Lithos, 9, 39–54.

——— (1978) Lapis lazuli from Baffin island – a precambrian meta-evaporite. Lithos, 11, 37–60.

Ishibashi, H., Arakawa, M., Ohi, S., Yamamoto, J., Miyake, A., and Kagi, H. (2008) Relationship between Raman spectral pattern and crystallographic orientation of a rock-forming mineral: A case study of $Fo_{89}Fa_{11}$ olivine. Journal of Raman Specatroscopy, 39, 1653–1659.

Johnson, E., Ferrer, J., and Chadderton, L.T. (1978) Radiolytic radiation damage of sodalite. Physica status solidi (a), 49, 585–591.

Jugo, P.J., Luth, R.W., and Richards, J.P. (2005) Experimental data on the speciation of sulfur as a function of oxygen fugacity in basaltic melts. Geochimica et Cosmochimica Acta, 69, 497–503.

Klimm, K. and Botcharnikov, R.E. (2010) The determination of sulfate and sulfide species in hydrous silicate glasses using Raman spectroscopy. American Mineralogist, 95, 1574–1579.

Kotelnikov, A.R., Kovalskii, A.M., and Suk, N.I. (2005) Experimental study of sodalite solid solutions with chlorine-sulfur isomorphic anion substitution. Geochemistry International, 43, 544–558.

Lazzeri, M. and Mauri, F. (2003) First principles calculation of vibrational Raman spectra in large systems: signature of small rings in crystalline SiO_2. Physical Review Letters, 90, 36401–36404.

Lede, B., Dermortier, A., Gobeltz-Hautecoeur, N., Lelieur, J.-P., Picquenard, E., and Duhayon, C. (2007) Observation of the υ_3 Raman band of S_3^- inserted into sodalite cages. Journal of Raman Spectroscopy, 38, 1461–1468.

Löwdin, P.-O. (1977) On the nonorthogonality problem. Advances in Quantum Chemistry, 5, 185–199.

Markl, G., Marks, M.A.W., Schwinn, G., and Sommer, H. (2001) Phase equilibrium constraints on intensive crystallization parameters of the Ilímaussaq Complex, South Greenland. Journal of Petrology, 42, 2231–2258.

Markl, G., Marks, M.A.W., and Frost, B.R. (2010) On the Controls of oxygen fugacity in the generation and crystallization of peralkaline melts. Journal of Petrology, 51, 1831–1847.

Merlino, S. (1984) Feldspathoids: Their average and real structures. In W.L. Brown, Ed., Feldspars and Feldspathoids, p. 435-470. Reidel, Dordrecht, The Netherlands.

Mohanan, K., Sharma, S.K., and Bishop, F.C. (1993) A Raman spectral study of forsterite-monticellite solid solutions. American Mineralogist, 78, 42–48.

Mori, R.A., Paris, E., Giuli, G., Eeckhout, S.G., Kavicic, M., Zitnik, M., Bucar, K., Pettersson, L.G.M., and Glatzel, P. (2009) Electronic structure of sulfur studies by X-ray absorption and emission spectroscopy. Analytical Chemistry, 81, 6516–6525.

Nagashima, S. and Katsura, T. (1973) The solubility of sulfur in Na_2O-SiO_2 melts under various oxygen partial pressures at 1100, 1250, and 1300 °C. Bulletin of the Chemical Society of Japan, 46, 3099–3103.

Perdew, J.P. and Zunger, A. (1981) Self-interaction correction to density-functional approximations for many-electron systems. Physical Review B, 23, 5048–5079.

Perdew, J.P., Burke, K., and Ernzerhof, M. (1996) Generalized gradient approximation made simple. Physical Review Letters, 77, 3865–3868.

Remond, G., Myklebust, R., Fialin, M., Nockolds, C., Phillips, M., and Roques-Carmes, C. (2002) Decomposition of wavelength dispersive X-ray spectra. Journal of Research of the National Institute of Standards and Technology, 107, 509–529.

Schilling, J., Frost, B.R., Marks, M.A.W., Wenzel, T., and Markl, G. (2011) Fe-Ti-oxide-silicate (QUIlF-type) equlilibria in feldspathoid-bearing systems. American Mineralogist, 96, 100–110.

Segall, M.D., Shah, R., Pickard, C.J., and Payne, M.C. (1996) Population analysis of plane-wave electronic structure calculations of bulk materials. Physical Review B, 54, 16317–16320.

Stormer, J.C. and Carmichael, I.S.E. (1971) The free energy of sodalite and the behavior of chloride, fluoride and sulfate in silicate magmas. American Mineralogist, 56, 292–306.

Suk, N.I., Kotelnikov, A.R., and Kovalskii, A.M. (2007) Mineral Thermometry and the Composition of Fluids of the Sodalite Syenites of the Lovozero Alkaline Massif. Petrology, 15, 441–458.

Taylor, B.E. (1986) Magmatic volatiles: Isotopic variation of, C, H, and S. In J.W. Valley, H.P. Taylor Jr., and J.R. O'Neil, Eds., Stable Isotopes In High-Temperature Geological Processes, 16, p. 185–225. Reviews in Mineralogy and Geochemistry, Mineralogical Society of America, Chantilly, Virginia.

van Peteghem, J.K. and Burley, B.J. (1963) Studies on solid solution between sodalite, nosean, and hauyne. The Canadian Mineralogist, 7, 808–813.

Wellman, T.R. (1970) The stability of sodalite in a synthetic syenite plus aqueous chloride fluid system. Journal of Petrology, 11, 49–72.

Wilke, M., Klimm, K., and Kohn, S.C. (2011) Spectroscopic studies on sulfur speciation in synthetic and natural glasses. In H. Behrens and J.D. Webster, Eds., Sulfur in Magmas and Melts: Its importance for natural and technical processes, 73, p. 41–73. Reviews in Mineralogy and Geochemistry, Mineralogical Society of America, Chantilly, Virginia.

Wulff-Pedersen, E., Neumann, E.-R., Burke, E.A.J., Vannucci, R., Bottazzi, P., Ottolini, L., Gjønnes, J., and Hansen, V. (2000) Origin and structural character of hauyne ss. in spinel dunit xenoliths from La Palma, Canary Islands. American Mineralogist, 85, 1397–1405.

Manuscript received October 24, 2011
Manuscript accepted May 20, 2012
Manuscript handled by Don Baker